JOURNAL OF Materials CHEMISTRY

A two-dimensional radical salt based upon BEDT-TTF and the dimeric, magnetic anion $[Fe(tdas)_2]_2^{2-}$: $(BEDT\text{-}TTF)_2[Fe(tdas)_2]$ (tdas = 1,2,5-thiadiazole-3,4-dithiolate)

Paola Deplano,[a] Laura Leoni,[a] Maria Laura Mercuri,*[a] John A. Schlueter,*[b] Urs Geiser,[b] Hau H. Wang,[b] Aravinda M. Kini,[b] Jamie L. Manson,[b] Carlos J. Gómez-García,[c] Eugenio Coronado,[c] H.-J. Koo[d] and M.-H. Whangbo[d]

[a]*Dipartimento di Chimica Inorganica ed Analitica, S.S. 554, Bivio per Sestu, I09042 Monserrato, Cagliari, Italy. E-mail: Mercuri@unica.it*
[b]*Materials Science Division, Argonne National Laboratory, Argonne IL 60439-4831, USA. E-mail: JASchlueter@anl.gov*
[c]*Instituto de Ciencia Molecular, Universidad de Valencia, Dr. Moliner 50, 46100 Burjasot, Spain*
[d]*Department of Chemistry, North Carolina State University, Raleigh NC 27695-8204, USA*

Received 8th May 2002, Accepted 18th September 2002
First published as an Advance Article on the web 29th October 2002

In an attempt to synthesize new synthetic metals which couple magnetic properties to conductivity, we prepared the novel salt $(BEDT\text{-}TTF)_2[Fe(tdas)_2]$ [BEDT-TTF = bis(ethylenedithio)tetrathiafulvalene, hereafter referred to as ET; tdas = 1,2,5-thiadiazole-3,4-dithiolate] by the electrocrystallization technique. The crystal structure of this compound, as determined by single crystal X-ray diffraction, contains conducting, organic ET layers separated by dimerized, magnetic $[Fe(tdas)_2]_2^{2-}$ anions. Due to the magnetic insulating ground electronic state of the ET layer, thermally activated conductivity is observed, with a room temperature value of about 1 S cm^{-1}. This salt was also characterized by EPR spectroscopy, dc magnetization measurements and Raman spectroscopy. The electronic structure of the ET layers was investigated by extended Hückel tight-binding calculations, and the spin exchange interactions of the ET and $[Fe(tdas)_2]^-$ layers were examined by spin-dimer analysis.

Introduction

Hybrid molecular solids which couple magnetic or optical properties to conductivity have increasingly been a focus of materials chemists because of the possibility that they may result in materials with novel physical properties leading to new applications.[1–7] Molecular charge-transfer salts are one promising class of such materials. The BEDT-TTF [bis(ethylenedithio)tetrathiafulvalene; hereafter written as ET] electron-donor molecule is well known for its ability to form conducting salts with a large variety of counteranions.[8,9] This molecule is a component of the majority of known organic superconductors and a large number of metallic and semiconducting salts, including the first superconductors with paramagnetic centers[10] and the first molecular metallic ferromagnet.[3] Salts of ET typically form two-dimensional layered structures in which conducting sheets of ET cation radicals are separated by layers of charge-compensating anions. We have thus chosen to study these conductive ET sheets as components of multifunctional solids.

As acceptor molecules, metal dithiolene complexes are of interest because of their ability to form (super)conducting[11] and magnetic salts.[12] We have selected to study planar metallodithiolenes, such as the $[M(dmit)_2]^{n-}$ (dmit = 1,3-dithiole-2-thione-4,5-dithiolate; M = Ni, Pd; $0 < n < 2$) systems and analogs, where peculiar conducting, magnetic, and optical properties have been observed.[13] We are mainly interested in modifying the heteroatoms (N, S, Se) in the periphery of the dmit ligand,[14,15] as well as the metal (Ni, Fe, *etc.*) to study the effect of such variations on the properties of the molecules themselves and on the corresponding materials.

In this regard, the $[Fe(tdas)_2]^-$ (tdas = 1,2,5-thiadiazole-3,4-dithiolate) anion, which contains N-atoms in the peripheral pentatomic ring of the dithiolene system and exhibits peculiar magnetic properties, is attractive as a component of multifunctional molecular solids. A previous report[16] on TBA[Fe(tdas)$_2$] (TBA = tetrabutylammonium) shows that the anion is present as a centrosymmetric dimer, and that the Fe^{3+} coordination sphere exhibits a distorted five-coordinate pyramidal structure. Unusual re-entrant behavior has been reported in the TBA[Fe(tdas)$_2$] salt,[16,17] where the same crystallographic phase has been observed both below 182 and above 232 K, while in the intermediate temperature regime, a second phase is present. Two salts of $(TTF)_x[Fe(tdas)_2]$ (TTF = tetrathiafulvalene) have been also described.[18] Both are semiconductors; for $x = 2$, the compound exhibits a thermally activated magnetic behavior, while for $x = 3/2$, a Curie-type behavior has been observed. More recently, the X-ray crystal structure and magnetic susceptibility of $(TTF)_2[Fe(tdas)_2]$ indicate that this structure possesses antiferromagnetic $[Fe(tdas)_2]_2^{-2}$ dimers and co-existing delocalized and localized unpaired electrons. An anomaly was observed in the magnetic susceptibility between 80 and 96 K, but no evidence for a re-entrant transition was found.[19] The 1 : 1 $(BETS)_2[Fe(tdas)_2]_2$ [BETS = bis(ethylenedithio)tetraselenafulvalene] salt, which contains segregated columns of dimerized BETS cations and columns of dimerized $[Fe(tdas)_2]$ anions, has recently been reported to exhibit metallic behavior above 200 K.[20]

The ET electron-donor molecule contains eight sulfur atoms (twice the number of TTF) and an extended π-system. Due in part to these features, ET-based charge-transfer salts have led to more two-dimensional metals than have their TTF

 DOI: 10.1039/b204435h

counterparts. ET has thus proven to be a much better building block for layered molecular-based metals and superconductors than TTF. For this reason, we have chosen to crystallize the ET counterpart of $(TTF)_2[Fe(tdas)_2]$ and compare the properties of these two salts. Herein, we report the synthesis of $(ET)_2[Fe(tdas)_2]$ and compare the structure and physical properties of this salt to those previously reported for $(TTF)_2[Fe(tdas)_2]$.

Experimental

Synthesis

ET was prepared as previously described[21,22] and recrystallized from chloroform prior to use. $TBA[Fe(tdas)_2]$ was prepared as reported earlier.[23] Black plate-like crystals of $(ET)_2[Fe(tdas)_2]$ were grown by using previously described electrocrystallization techniques:[24,25] $TBA[Fe(tdas)_2]$ (35 mg) was added to both chambers of an H-cell. ET (7.5 mg) was loaded into the anode chamber. The crystallization solvent, benzonitrile (7.5 mL), was then added to each chamber of the H-cell and the cell backfilled with argon gas. A current density of 0.13 μA cm^{-2} was initially applied and gradually increased over a period of 6 days to 0.25 μA.cm^{-2}, at which time crystallization of black crystals commenced on the electrode surface. Crystals were grown at 25 °C on platinum wire electrodes for a period of 50 days. The best $(ET)_2[Fe(tdas)_2]$ crystals grew when benzonitrile was used as the solvent, although even these proved to be heavily twinned. For this reason, we denote individual crystals as 'single' in quotes in the following text. Even poorer quality crystals were obtained when 1,1,2-trichloroethane was employed as the crystallization solvent.

Crystal structure determination

The structure of $(ET)_2[Fe(tdas)_2]$ was determined at 298 K by single crystal X-ray diffraction using a Siemens SMART® single crystal X-ray diffractometer equipped with a CCD-based area detector and a sealed-tube X-ray source. Further details are available in the CIF file deposited as electronic supplementary information (ESI).

Crystal data: $(S_8C_{10}H_8)_2Fe(S_3N_2C_2)_2$, $M_w = 1121.71$, monoclinic, space group $P2_1/c$ (no. 14), $a = 11.6342(12)$, $b = 4.1608(5)$, $c = 40.513(5)$ Å, $\beta = 98.070(6)°$, $V = 1941.7(4)$ $Å^3$, $T = 298(2)$ K, $Z = 2$, $\lambda = 0.71073$ Å, $\rho_{calcd} = 1.918$ g cm^{-1}, $\mu = 1.603$ mm^{-1}, reflections collected = 12582, independent reflections = 4620, $R_1 = 0.192$, $wR_2 = 0.488$. See below for a discussion of the crystal quality and extra crystallographic complications.

CCDC reference number 156842.

See http://www.rsc.org/suppdata/jm/b2/b204435h/ for crystallographic data in CIF or other electronic format.

Physical properties

A microcrystalline sample of $(ET)_2[Fe(tdas)_2]$ was studied between 300 and 100 K using an IBM ER200 x-band (9.49 GHz) EPR spectrometer equipped with a VT4111 liquid nitrogen temperature controller.

Dc conductivity measurements over the range 80–300 K were performed by the two contacts method (due to the small size of the crystals) in two different 'single' crystals, giving reproducible results in both samples. Contacts between the crystals and platinum wires (25 μm diameter) were made using graphite paste. The samples were cooled using the cryostat of the SQUID susceptometer (see below). The cooling and warming rate was 1 K min^{-1} and the results were, within experimental error, identical in the cooling and warming sweeps.

Raman spectra of a 'single' crystal of $(ET)_2[Fe(tdas)_2]$ were obtained at room temperature using a Raman microscope (BX 40, Olympus) spectrometer (ISA xy 800) equipped with He–Ne ($\lambda = 632.8$ nm) and Ar ($\lambda = 514.5$ nm) lasers. The scattering peaks were calibrated against a Si standard ($\nu = 520$ cm^{-1}). A typical spectrum was collected every 500 s with a 1 cm^{-1} resolution and was averaged over 5 scans. No sample decomposition was observed during the experiments.

Variable temperature magnetic susceptibility measurements were carried out in the temperature range 2–300 K at an applied magnetic field of 0.1 T on polycrystalline samples with a Quantum Design MPMS-XL-5 SQUID magnetometer. The experiment was performed with three different cooling rates: fast (10 K min^{-1}), intermediate (1 K min^{-1}) and slow (0.5 K min^{-1}). The magnetic measurements were carried out whilst warming the sample. The magnetization curves were identical for the three cooling rates. The susceptibility data were corrected for the sample holder, previously measured using the same conditions, and for the diamagnetic contributions of the salt, as deduced using Pascal's constant tables.

Results and discussion

Crystal structure

For the crystal structure determination of $(ET)_2[Fe(tdas)_2]$, a number of crystals were examined, but none were found to be untwinned. Furthermore, they all exhibited diffuse diffraction maxima (see below), indicating further crystallographic complications. Finally, a twinned crystal was selected where at least half of the diffracting power was concentrated in one twin domain. The remaining peaks arose from other domains, and we could not discern a specific twin law that could have been applied to correct the observed diffraction intensities. The provisional structure of this crystal is described here. While details of bond geometry are certainly not satisfactorily defined by data obtained from such a poor quality sample, the overall structural features are clearly recognizable.

Fig. 1(a) and (b) show the atom numbering used for the ET electron-donor molecules and the $[Fe(tdas)_2]^-$ anions, respectively. As is the case with almost all ET cation radical salts,[8,9] the ET donor molecules are packed into layers (*ab*-plane), while the anions are located between adjacent layers [see Fig. 2(a)]. As illustrated in Fig. 2(b), the ET molecules form uniform stacks along the *b*-axis, and are tilted 20.6° with regard to the stacking axis. The tilts of adjacent stacks have opposite senses, forming a herringbone-type structure. This packing type is commonly referred to as θ-type.[26] The dihedral angle between ET molecules in adjacent stacks is thus 139°. This is significantly larger than in most other θ-type salts.

The ET molecules in $(ET)_2[Fe(tdas)_2]$ form nominally uniform stacks (although short range dimerization due to the anion superstructure cannot be excluded) with no short (<3.65 Å) intermolecular sulfur–sulfur contacts within the

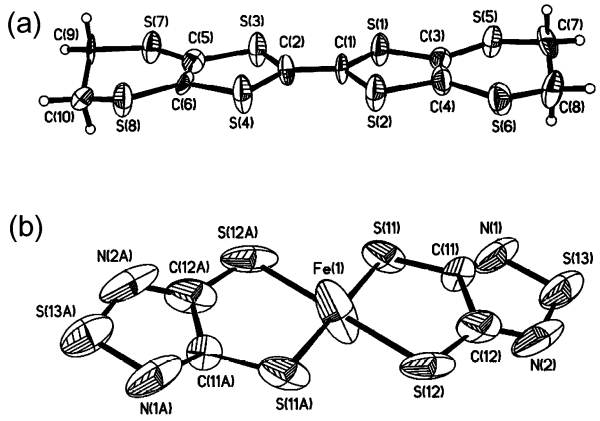

Fig. 1 Atom numbering used for (a) the ET electron-donor molecules and (b) the $[Fe(tdas)_2]^-$ anions of $(ET)_2[Fe(tdas)_2]$.

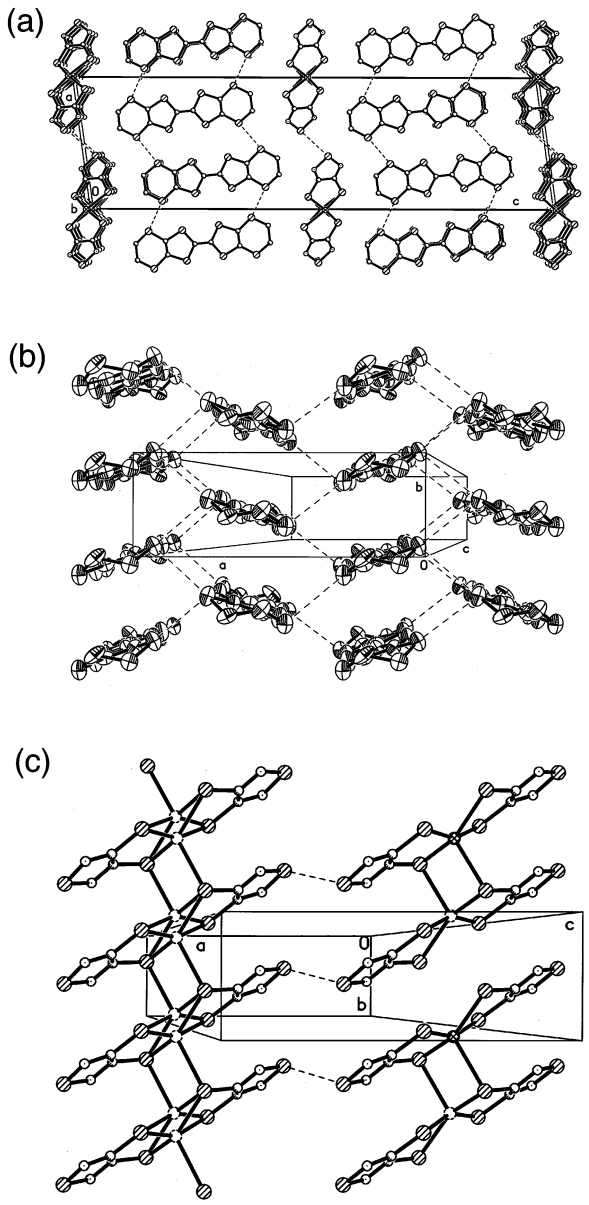

Fig. 2 (a) Projection of the crystal structure of $(ET)_2[Fe(tdas)_2]$ along the *b*-axis. (b) θ-Type packing motif of the ET molecules in the electron-donor layer. Intermolecular S···S contacts shorter than 3.65 Å are illustrated as dashed lines. (c) The $[Fe(tdas)_2]^-$ anion layer, showing on the left-hand side a uniform stack with disordered iron atoms and on the right-hand side a plausible dimerized superstructure (short range order only). The dashed lines indicate the 3.344 Å intermolecular contacts between the terminal, S(13), sulfur atoms.

stacks. This is in contrast to the $(TTF)_2[Fe(tdas)_2]$ structure, which contains an ABCB-type stacking arrangement and short intra-stack sulfur–sulfur interactions.[19] Although inter-stack sulfur–sulfur contacts are observed in $(TTF)_2[Fe(tdas)_2]$, the extended sulfur framework of the ET molecule allows for increased side-to-side sulfur–sulfur interactions in the $(ET)_2[Fe(tdas)_2]$ structure and the formation of a distorted honeycomb-type network. Sulfur···sulfur contacts shorter than 3.65 Å are observed between ET molecules in adjacent stacks. Each of these contacts are between sulfur atoms in the outer six-membered rings: S(5)···S(7) (3.60 and 3.63 Å) and S(6)···S(8) (3.64 Å). The increased importance of side-by-side interactions is a general trend when comparing ET with TTF salts.

The $[Fe(tdas)_2]^-$ anions also stack along the *b*-axis [see Fig. 2(c)]. They are located near the cell origin, but the iron atom position is offset from the inversion center, with half occupancy. This offset gives the iron center a fifth ligand, a sulfur atom of an adjacent anion, and the coordination is square pyramidal (equatorial Fe–S bond lengths ~2.15 Å, axial bond length ~2.72 Å). A plausible stacking pattern is shown on the right-hand side of Fig. 2(c), where at least a local order is assumed, with a 2*b*-superstructure leading to dimerized $[Fe(tdas)_2]_2^{-2}$ anions. However, this order is not long range (especially not in the *a*- and *c*-directions), consistent with the observation of diffuse scattering intensity in reciprocal lattice sheets with half-integer *k* Miller indices. The $[Fe(tdas)_2]^-$ anions are linked in a head-to-tail fashion by short (3.344 Å) intermolecular S···S contacts [see Fig. 2(c)]. Hydrogen-bonding contacts are observed between the hydrogen atoms of the ET molecules and both the sulfur [S(11)···H(7a) = 2.89, S(13)···H(8a) = 2.93 Å] and nitrogen [N(2)···H(10b) = 2.55 Å] atoms of the $[Fe(tdas)_2]^-$ anion.

Physical properties

A Raman study of a single crystal of $(ET)_2[Fe(tdas)_2]$ was performed in order to gain information on the degree of charge transfer in this salt. An approximately linear dependence between the degree of charge transfer and the Raman-active C=C stretching frequencies in insulating, conducting, and superconducting ET-based salts has previously been established.[27] Raman spectra of a single crystal of $(ET)_2[Fe(tdas)_2]$ carried out at room temperature using a Raman microscope spectrometer equipped with He–Ne (λ = 632.8 nm) and Ar (λ = 514.5 nm) lasers are reported in Fig. 3. When using the He–Ne laser, the Raman spectrum is dominated by the anion (resonance enhancement) and no peaks can be assigned unambiguously in the 1400–1550 cm^{-1} range, where the two totally symmetrical (Raman-active) C=C stretching modes are expected. The spectrum obtained using the Ar laser shows a peak at 1469 cm^{-1}. This peak can be assigned to the totally symmetrical C=C stretching vibration, ν_4, of the ET molecule and is consistent with a 2 : 1 charge-transfer salt in which the ET molecules possess an oxidation state of +0.5, in agreement with the X-ray results.

The EPR spectrum consists of two components. A pronounced peak with a linewidth of about 55 G at room temperature is assigned to the $(ET)_2^+$ radical cation. This linewidth is typical of ET salts with a θ-type packing motif.[28] As illustrated in Fig. 4(a), the linewidth of the $(ET)_2^+$ resonance decreases with decreasing temperature from 55 G at 300 K to 41 G at 100 K. The relative spin susceptibility increases with decreasing temperature, although there is a notable discontinuity in the spin susceptibility between 260 and 170 K.

Secondly, a very broad peak with room temperature linewidth of about 1500 G can be attributed to the $[Fe(tdas)_2]^-$ anion. As illustrated in Fig. 4(b), the linewidth of this resonance broadens significantly with decreasing temperature

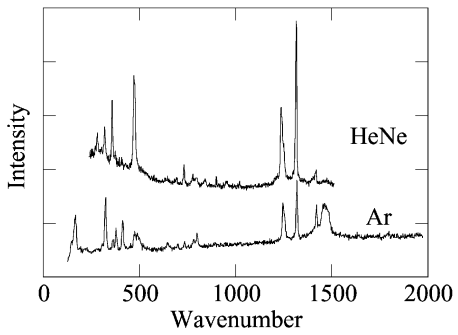

Fig. 3 Raman spectra of $(ET)_2[Fe(tdas)_2]$ obtained at room temperature from a single crystal using He–Ne (λ = 632.8 nm, dotted line) and Ar (λ = 514.5 nm, solid line) lasers.

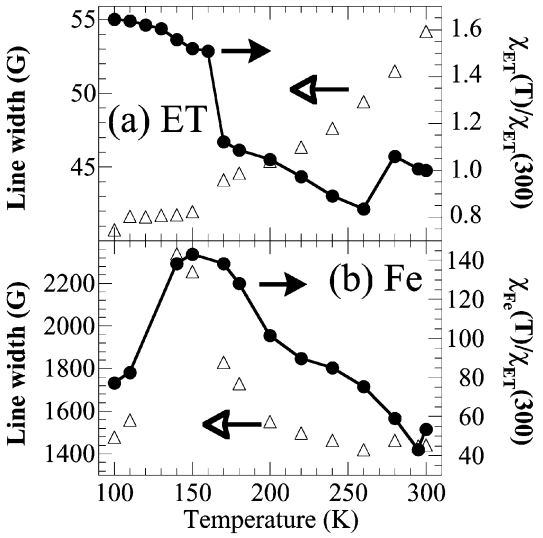

Fig. 4 Temperature-dependent EPR linewidth (△) and spin susceptibility (●) of (a) $(ET)_2^+$ (the solid line is a guide to the eye which emphasizes the re-entrant region as viewed in the spin susceptibility) and (b) Fe^{3+} in $(ET)_2[Fe(tdas)_2]$.

to 2300 G at 140 K. Between 120 and 130 K, the $[Fe(tdas)_2]^-$ contribution is distorted and cannot be fitted satisfactorily. Below 110 K, the linewidth decreases to about 1800 G. In general, the spin susceptibility increases with decreasing temperature. However, there is also a notable decrease in the spin susceptibility of the $[Fe(tdas)_2]^-$ component below 150 K. The Fe^{3+} contribution to the spin susceptibility is about two orders of magnitude greater than the contribution from $(ET)_2^+$.

The discontinuity of the spin susceptibility between approximately 170 and 260 K in both the $(ET)_2^+$ and $[Fe(tdas)_2]^-$ components is reminiscent of the discontinuity in the paramagnetic susceptibility previously reported for TBA[Fe(tdas)$_2$].[16] In this case, the anomaly is attributed to a re-entrant phase transition associated with a structural rearrangement of the $[Fe(tdas)_2]^-$ anions. From the EPR data, it appears likely that a similar, minor, re-entrant rearrangement of the $[Fe(tdas)_2]^-$ anion also occurs in the $(ET)_2[Fe(tdas)_2]$ salt. The rearrangement of the $[Fe(tdas)_2]^-$ anion must cause a small compensating adjustment of the ET molecules, which is observed in the discontinuous spin susceptibility of the EPR signal of the $(ET)_2^+$ radical. Hydrogen bonding between the ET layer and the $[Fe(tdas)_2]^-$ anions must be responsible for the subtle rearrangement of the ET molecules in response to the re-entrant structural modification of the anion layer.

The bulk, static molar susceptibility (χ_m) of the $(ET)_2[Fe(tdas)_2]$ salt per $[Fe(tdas)_2]_2^{2-}$ dimer, *i.e.* for the formula $(ET)_4[Fe(tdas)_2]_2$, is plotted in Fig. 5. Reminiscent of the spin susceptibility of the Fe^{3+} component observed by EPR, χ_m shows a smooth increase when cooling the sample, reaching a very broad maximum centered at about 145 K. Below this temperature, the susceptibility decreases and reaches a rounded minimum at 28 K and a divergence at low temperatures. The $\chi_m T$ product displays a continuous decrease from approximately 1.8 emu K mol^{-1} at room temperature to a value close to zero at 2 K. The decrease in the $\chi_m T$ plot, as well as the maximum in the χ_m plot, indicate the presence of a dominant antiferromagnetic coupling between the Fe(III) centers in the salt (although a contribution from the organic radical cannot be excluded). From the $\chi_m T$ value at room temperature (1.8 emu K mol^{-1}), we can conclude that the spin ground state of the Fe(III) ions must be 3/2, as expected for a high spin configuration in a d^5 ion with square pyramidal coordination and in agreement with the spin state found in the TBA and

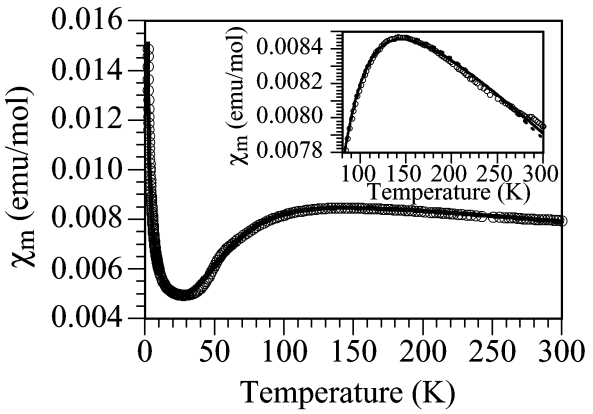

Fig. 5 Thermal variation of the magnetic susceptibility for the salt $(ET)_2[Fe(tdas)_2]$. The lines show the best fit to a model of interacting $S = 3/2$ dimers for the anionic sublattice plus a regular antiferromagnetic $S = 1/2$ chain model with (solid line) and without (dotted line) interchain interactions (see text) for the ET sublattice. Inset: the high temperature region.

TTF salts of the same anion.[16,19] As is also the case for the TTF salt,[19] no discontinuity in the static susceptibility is observed. For the ET salt, the EPR spectrum of the radical cation is sensitive to the re-entrant phase transition because it is not hidden by the larger moment of the $[Fe(tdas)_2]^-$ anions, as it is in the static measurement.

The 'single' crystals of $(ET)_2[Fe(tdas)_2]$ synthesized so far are too small for traditional four-probe conductivity studies. Thus, we have measured the conductivity (σ) of single crystals by a two-probe method. Although the absolute value of the conductivity cannot be measured accurately by this method, the thermal behavior is thought to be correct. The data obtained from two independent crystals, both on warming and cooling scans, were reproducible. A typical conductivity curve is illustrated in Fig. 6 on a logarithmic scale as a function of inverse temperature (1000/T). The room temperature conductivity of about 1 S cm^{-1} is relatively high. As $(ET)_2[Fe(tdas)_2]$ is cooled, its conductivity decreases rapidly to about 10^{-4} S cm^{-1} at 100 K. Below this temperature, the resistance becomes higher than the impedance of the voltmeter. An important point that can be seen in this figure is that there are three different semiconducting regimes (straight lines whose slopes are proportional to the activation energies). The fits of these three regimes give activation energies of 104(1), 155(4), and 104(2) meV in the high (300–250 K), medium (250–160 K) and

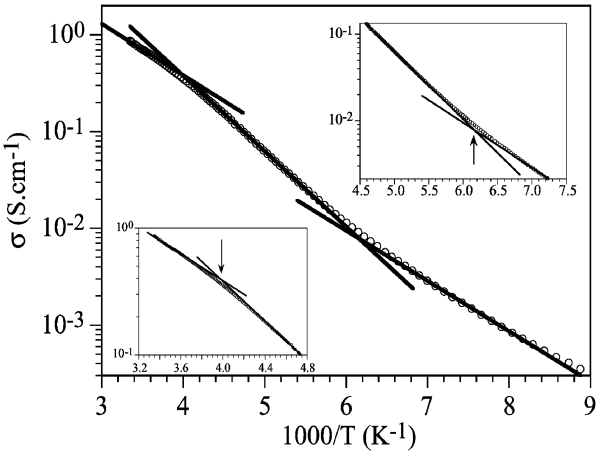

Fig. 6 Themal dependence of the dc conductivity (logarithmic scale) of the salt $(ET)_2[Fe(tdas)_2]$ as a function of 1000/T. Insets show the changes in the slopes at 1000/T values of about 4 and 6.2 (250 and 160 K, respectively).

low (160–100 K) temperature regimes, respectively. The intersects of the straight lines describing each regime show that the temperatures of the transitions between these regimes are approximately 250 and 160 K (see insets in Fig. 6).

Although the changes in the slopes of the conductivity plot are very slight, the large number of measured points (Fig. 6 only shows 10% of the acquired data), the reproducibility of the changes found in two different crystals in both cooling and warming scans, and the relative change of the slope in both transitions (about 50% of the previous values) support the idea that these changes are intrinsic to the samples and not an artifact. The values found for the activation energies suggest that the transition observed at low temperature (160 K) corresponds to a "re-entrant" transition to the high temperature phase (as the activation energy comes back to its original value at high temperatures). Note that the transition temperatures are very close to those observed in the EPR experiments and in the TBA^+ salt of the same anion.[16]

It has been shown that a broad minimum in the overlap integral occurs when the dihedral angle between the molecular planes of ET molecules in adjacent stacks is near 140° in θ-type salts.[26] The observation that $(ET)_2[Fe(tdas)_2]$ exhibits semiconductive behavior is consistent with the fact that many θ-type salts with dihedral angles greater than 125° are paramagnetic insulators, even at room temperature.[26]

The room temperature conductivity of $(ET)_2[Fe(tdas)_2]$ is about two orders of magnitude higher than that reported for $(TTF)_2[Fe(tdas)_2]$.[19] Although both materials are semiconductors, the activation energy of $(ET)_2[Fe(tdas)_2]$ is lower by a factor of two. The improved electrical conductivity of $(ET)_2[Fe(tdas)_2]$ is attributed to the extended sulfur framework of the ET molecule and its ability to form a more two-dimensional conductive network through inter-stack sulfur–sulfur interactions.

Electronic structure and spin exchange interactions

We examined the electronic structure of a single ET layer of $(ET)_2[Fe(tdas)_2]$ using the extended Hückel tight-binding method.[29,30] A single ET layer has four ET molecules per unit cell. The two highest occupied bands, shown in Fig. 7, have contributions primarily from the HOMOs of the ET molecules. With the oxidation state $(ET)_2^+$, there are only three electrons to fill the two bands. Thus, if electron correlation (*i.e.* electron–electron repulsion) is neglected, the Fermi level would be as indicated in Fig. 7. The band structure shows no band gap and, hence, predicts $(ET)_2[Fe(tdas)_2]$ to be metallic. This prediction does not agree with experiment, so electron correlation must be important in the ET layers of $(ET)_2[Fe(tdas)_2]$ and the ground state of each ET layer should be magnetic insulating[31] instead of metallic. A molecular view of the magnetic insulating state is that every dimer cation $(ET)_2^+$ keeps an unpaired spin. The highest two occupied orbitals of an $(ET)_2^+$ dimer cation, ψ_+ and ψ_-, are the bonding and antibonding combinations of the two HOMOs, respectively. Thus, as illustrated in Fig. 8(a), each $(ET)_2^+$ dimer cation has the electron configuration $(\psi_+)^2(\psi_-)^1$ in the magnetic insulating state. The ψ_+ and ψ_- levels give rise to two bands due to the interactions between $(ET)_2^+$ dimers, with the lower band from ψ_+ and the upper one from ψ_-. The ground state of each ET layer is metallic when the upper band is half-filled, as shown in Fig. 8(b), where each level of the lower half is doubly filled while that of the upper half is vacant.[31] The ground state of each ET layer is magnetic insulating when the upper band is half-filled, as shown in Fig. 8(c), where all the levels are singly filled.[31]

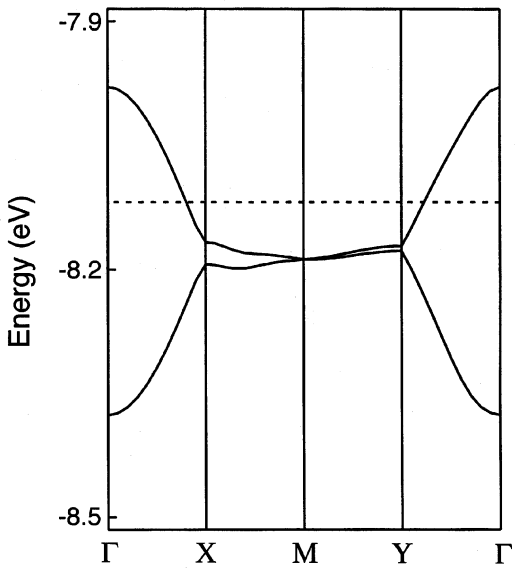

Fig. 7 Dispersion relations of the two highest occupied bands of an isolated ET layer, where the Fermi level (dashed line) is given assuming that the ground state of the ET layer is metallic.

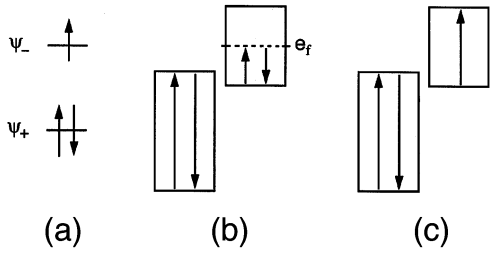

Fig. 8 (a) The two highest occupied levels, ψ_+ and ψ_-, of an $(ET)_2^+$ dimer cation, which are the bonding and antibonding combinations of the two HOMOs, respectively. (b) Schematic representation of the band filling for the metallic state of an isolated cation layer of $(ET)_2[Fe(tdas)_2]$. (c) Schematic representation of the band filling for the magnetic insulating state of an isolated cation layer of $(ET)_2[Fe(tdas)_2]$.

We now turn our attention to the spin exchange interactions in the ET layers of $(ET)_2[Fe(tdas)_2]$. To identify the spin monomers (*i.e.* the structural units containing an unpaired spin) of the ET layers, we calculated the HOMO–HOMO interaction energies $\beta_{ij} = <\psi_i|\boldsymbol{H}^{\text{eff}}|\psi_j>$ where ψ_i and ψ_j refer to the HOMOs of the ET molecules i and j, respectively, and $\boldsymbol{H}^{\text{eff}}$ is the effective Hamiltonian of the extended Hückel method. The β_{ij} values are summarized in Fig. 9(a), which shows that the inter-stack interactions are stronger than the intra-stack interactions and that two different kinds of inter-stack interaction occur. As indicated by ellipses in Fig. 9(b), we chose the spin monomers as the ET pairs with the largest β_{ij} value. [As can be seen from Fig. 9(a), an alternative set of spin monomers could be chosen]. For a number of magnetic solids, it has been demonstrated[32–35] that trends in spin exchange interactions are well reproduced in terms of the spin–orbital interaction energies calculated for their spin dimers using the extended Hückel method. Here, spin dimers refer to structural units containing two adjacent spin sites. Therefore, for each ET layer of $(ET)_2[Fe(tdas)_2]$, the spin dimers are given by $[(ET)_2^+]_2$. The spin exchange parameter, J, for a given spin dimer consists of ferromagnetic and antiferromagnetic components, $J = J_F + J_{AF}$. Given that Δe is the spin–orbital interaction energy [*i.e.* the energy separation between the two highest singly occupied energy levels of a spin dimer, Fig. 10], the antiferromagnetic term, J_{AF} (<0), is related to Δe by $J_{AF} \propto -(\Delta e)^2$. In general, the ferromagnetic term, J_F (>0), is small and the spin exchange interaction becomes ferromagnetic (*i.e.* $J > 0$) when J_{AF} is negligibly small in magnitude. The spin–orbital interaction energies calculated for the ET layer of $(ET)_2[Fe(tdas)_2]$ are summarized in Fig. 9(b), where

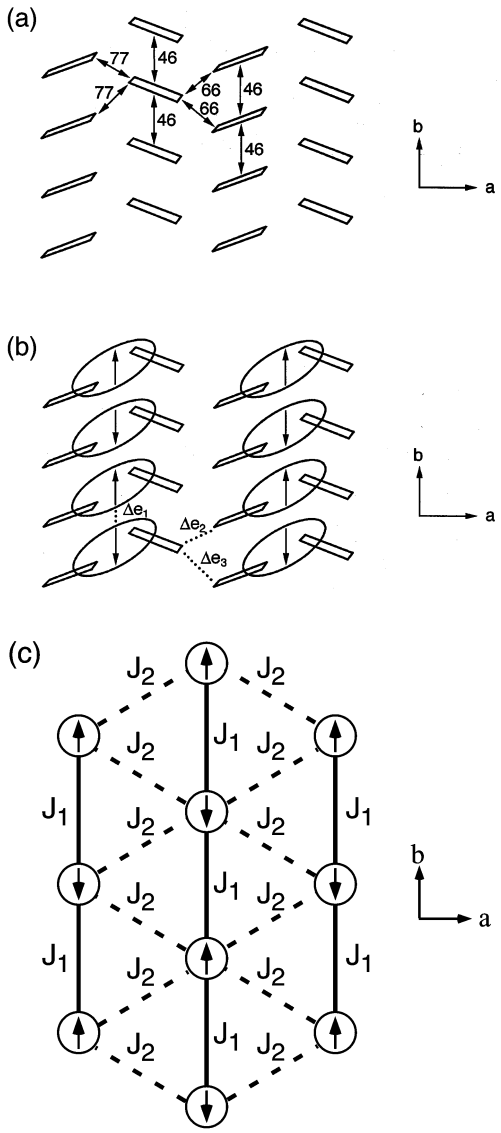

Fig. 9 (a) HOMO–HOMO interaction energies, β_{ij} (in meV), between adjacent ET molecules in a cation layer of $(ET)_2[Fe(tdas)_2]$. (b) Spin monomers in the cation layers of $(ET)_2[Fe(tdas)_2]$. The two ET molecules in each ellipse form a spin monomer. The spin–orbital interaction energies calculated for the three spin dimers (connected by the dotted lines) are as follows: $\Delta e_1 = 44$, $\Delta e_2 = 31$, and $\Delta e_3 = 28$ meV. (c) Schematic representation of the spin exchange pathways in a cation layer of $(ET)_2[Fe(tdas)_2]$, where J_1 and J_2 are the spin exchange parameters for the intra-chain and inter-chain interactions, respectively.

$\Delta e_1 > \Delta e_2 \approx \Delta e_3$. Thus, the magnetic structure of each ET layer is described in terms of interacting magnetic chains, as shown in Fig. 9(c), where J_1 and J_2 are the intra- and inter-chain spin exchange interactions, respectively.

Let us consider the spin exchange interactions in the $[Fe(tdas)_2]$ chains of $(ET)_2[Fe(tdas)_2]$, where each high spin Fe^{3+} site has three unpaired spins due to the square planar coordination of Fe^{3+}. In general, for a spin dimer that has M unpaired spins at each spin site, the spin exchange parameter J_{AF} is related to the average spin–orbital interaction energy, $<\Delta e>$,[34]

$$\langle \Delta e \rangle = \frac{1}{M^2} \sum_{\mu=1}^{M} \Delta \varepsilon_{\mu\mu} \quad (1)$$

where $\Delta \varepsilon_{\mu\mu}$, is the spin–orbital interaction energy associated with the magnetic orbitals, ϕ_μ, located at the two spin sites. In the $[Fe(tdas)_2]$ chains of $(ET)_2[Fe(tdas)_2]$, the $Fe(tdas)_2$ units (*i.e.* the spin monomers) are dimerized. Our calculations show that the spin–orbital interaction energies $<\Delta e>$ of the intra- and inter-dimer spin exchange interactions are 28 and 23 meV, respectively, thereby suggesting that the spin lattice of the $[Fe(tdas)_2]$ anions might be better described by alternating chains of $S = 3/2$ spin sites rather than by isolated dimers of S = 3/2 spin sites.

Analysis of the magnetic properties

In this section, we analyse the magnetic susceptibility of $(ET)_2[Fe(tdas)_2]$ from the viewpoint of the spin exchange interactions of the cation layers and the anion chains. Let us first assume that the magnetic susceptibility of $(ET)_2[Fe(tdas)_2]$ arises solely from the anion lattice. As it is not straightforward to determine the magnetic behavior of the anionic sublattice from the structural data, we have fitted the susceptibility curve of $(ET)_2[Fe(tdas)_2]$ using three different models: (i) a regular $S = 3/2$ antiferromagnetic chain,[36] (ii) an isolated $S = 3/2$ dimer, and (iii) an alternating $S = 3/2$ chain (using the molecular field approximation[37]). To these three models, the contribution of a small amount of paramagnetic impurity (in the form C/T) was added to reproduce the divergence at low temperatures. Nevertheless, none of the three models is able to satisfactorily reproduce the rounded maximum at about 145 K and the minimum at about 28 K. These unsuccessful attempts to fit the magnetic behavior of the $(ET)_2[Fe(tdas)_2]$ suggest that the cationic ET sublattice must also contribute to the magnetic moment of the salt, as also seems to occur in the TTF salt of this anion.[19] From the calculations of the spin exchange interactions (see above), we have tried to reproduce this contribution with a model of interacting $S = 1/2$ antiferromagnetic regular chains [Fig. 9(c)]. Nevertheless, in order to confirm the occurrence of the inter-chain interactions, we first used a simple regular chain model without any inter-chain interaction[38,39] and, secondly, a model of interacting regular chains. In this last case, the inter-chain interactions are reproduced with the molecular field approximation, as described below.

The combination of the three possible models for the anionic sublattice (isolated dimer, regular chain, and alternating chain) with the two possible models for the cationic sublattice (regular chain with or without inter-chain interactions) gives rise to a total of six possible models to reproduce the magnetic behavior of the $(ET)_2[Fe(tdas)_2]$ salt. We have tested the six models and found that those models where the anionic sublattice is reproduced with a regular $S = 3/2$ chain do not give good results. The other four possibilities offer similar results, although the models that consider an alternating $S = 3/2$ chain for the anionic sublattice are slightly better. Therefore, we can conclude that the anionic sublattice can be well reproduced with an alternating $S = 3/2$ chain, in agreement with the crystallographic data and the calculations of the spin exchange interactions (see above) which suggest a strong dimerization of the $[Fe(tdas)_2]^-$ chain.

The other important point concerns the contribution of the ET sublattice. In this case, both models (isolated and interacting regular antiferromagnetic $S = 1/2$ chains) produce similar results. This effect is probably due to the large number of parameters used, which prevent an accurate determination of their exact values and masks the effect of the variation of one or more of these parameters. Thus, the final results become very insensitive to the changes in the inter-chain exchange parameter, precluding any exact determination of the magnitude of the inter-chain interactions in the cationic sublattice. Attempts to reduce the number of adjustable parameters [by fixing the g value of the $(ET_2)^+$ radical to 2.0 and the $J_1(ET)/J_2(ET)$ ratio to 2, as indicated by the calculations] do not significantly improve the accuracy of the parameters.

Therefore, we finally reproduced the magnetic behavior of the $ET_2[Fe(tdas)_2]$ salt with an $S = 3/2$ alternating chain

for the anionic sublattice (χ_{Fe}) plus an interacting $S = 1/2$ regular antiferromagnetic chain for the ET sublattice (χ_{ET}) with eqn. 2

$$\chi_{exp} = \chi_{Fe} + \chi_{ET} \quad (2)$$

with

$$\chi_{Fe} = \frac{\chi_{id}}{1 - \left(\frac{2zJ_2(Fe)}{Ng^2\beta^2}\right)\chi_{id}} \quad (3)$$

where z is the number of magnetic nearest-neighbors ($z = 2$ in this case), J_2(Fe) is the inter-dimer exchange coupling and χ_{id} is the susceptibility of an isolated $S = 3/2$ dimer (eqn. 4),

$$\chi_{id} = \frac{Ng^2\beta^2}{kT}\frac{28e^{12x} + 10e^{6x} + 2e^{2x}}{7e^{12x} + 5e^{6x} + 3e^{2x} + 1} \quad (4)$$

with $x = J/kT$.

The contribution of the ET sublattice is reproduced with a model of interacting $S = 1/2$ regular antiferromagnetic chains (molecular field approximation):

$$\chi_{ET} = \frac{\chi_{ic}}{1 - \left(\frac{2zJ_2(ET)}{Ng^2\beta^2}\right)\chi_{ic}} \quad (5)$$

As before, z is the number of magnetic nearest-neighbors ($z = 2$ in this case), J_2(ET) is the inter-chain exchange coupling, and χ_{ic} is the susceptibility of an isolated $S = 1/2$ regular antiferromagnetic chains that can be approximated with the formula proposed by Hatfield *et al.*[39] (eqn. 6).

$$\chi_{ic} = 2\frac{Ng^2\beta^2}{kT} \times \frac{0.25 + 0.14995(|J|/kT) + 0.30094(|J|/kT)^2}{1 + 1.9862(|J|/kT) + 0.68854(|J|/kT)^2 + 6.0626(|J|/kT)^3} \quad (6)$$

The factor 2 introduced in eqn. 6 accounts for the fact that the spin carriers are dimers of ET molecules: $(ET_2)^+$ and the susceptibility plot (Fig. 5) is calculated per $[Fe(tdas)_2]_2^{2-}$ dimer and, therefore, there are 4 ET molecules [*i.e.* 2 $(ET_2)^+$ units] in the formula.

With eqn. 2, a very good fit is obtained in the whole temperature region with the following set of parameters: $g_{Fe} = 2.1(1)$, J_1(Fe) = −68(2) cm^{-1}, J_2(Fe) = -−3(5) cm^{-1}, $g_{ET} = 2.0$, J_1(ET) = −40(1) cm^{-1}, J_2(ET) = −19(6) cm^{-1}, and 1.2(1)% monomeric $S = 3/2$ impurity (solid line in Fig. 5). Note that the g value of the ET chain has been fixed to 2.0 to reduce the number of adjustable parameters. As indicated by the spin exchange calculations, the J_1/J_2 ratio is very close to 2 in the ET sublattice. However, this is not the case for the J_1/J_2 ratio in the anionic sublattice (that should be close to 1.5 after the calculations). The fact that the final fit is very insensitive to the inter-dimer exchange parameter (where the error is higher than the value itself), would explain this difference.

Finally, it is important to note that the models that consider the anionic lattice as isolated dimers and the models that consider the ET sublattice as isolated chains also produce quite good results. Thus, the model of interacting $S = 3/2$ dimers for the Fe sublattice plus isolated regular chains in the ET sublattice also gives very good results with the following set of parameters: $g_{Fe} = 2.08(8)$, J_1(Fe) = −65(1) cm^{-1}, J_2(Fe) = −9(4) cm^{-1}, $g_{ET} = 2.0$ (fixed), J_1(ET) = −51.0(2) cm^{-1}, and 1.2(1)% monomeric $S = 3/2$ impurity (dashed line in Fig. 5).

Therefore, although the best results are obtained with the interacting dimers and chains, the other possibilities (especially the isolated chains for the ET sublattice) cannot be totally excluded.

Note that the spin lattice of the cation layer [Fig. 9(c)] leads to spin frustration because each dimeric $(ET)_2^+$ unit has an equilateral triangle arrangement of spins. The Curie tail at low temperatures most likely arises from isolated ET^+ radicals due to crystal defects. This kind of contribution has already been observed in many other TTF-type radical salts.[40,41]

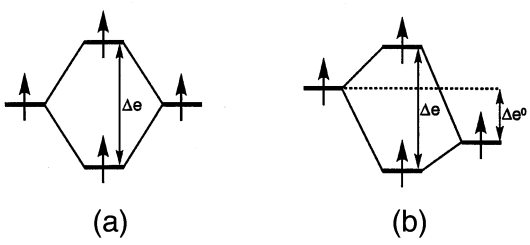

Fig. 10 (a) Spin–orbital interaction energy, Δe, of a spin dimer with two equivalent spin sites. (b) Spin–orbital interaction energy, $\Delta e - \Delta e^0$, of a spin dimer with two non-equivalent spin sites.

Concluding remarks

Crystals of the molecular-based conductor $(ET)_2[Fe(tdas)_2]$ have been grown through an electrocrystallization process. The two-dimensional structure contains layers of partially oxidized ET molecules separated by layers of dimerized, magnetic $[Fe(tdas)_2]_2^{2-}$ counterions. The ET layer exhibits thermally activated conductivity because the ground electronic state of each cation layer is magnetic insulating. Thus, in the $(ET)_2[Fe(tdas)_2]$ salt, unpaired electrons are present both in the cation layers and in the anion chains. To our knowledge, there is only one example of magnetic trimers used with TTF radicals[42] and two more recent examples of magnetic dimers used as counterions with TTF-type radical salts: (i) the anion $[Fe_2(ox)_5]^{4-}$ (ox = oxalate anion = $C_2O_4^{2-}$), which has been combined with the donors TTF,[43,44] TMTTF,[43,44] and ET[45] and (ii) the anion $[CrM(ox)(NCS)_8]^{4-}$ (M = Cr^{III}, Fe^{III}), which has only been combined with ET.[46,47] The discontinuity observed in the EPR spin susceptibility of $(ET)_2[Fe(tdas)_2]$ is reminiscent of that previously reported for $TBA[Fe(tdas)_2]$ (although opposite in sign). This transition, which is apparently structural in nature, will be probed in future studies. It should be noted that the $TTF_2[Fe(tdas)_2]$ salt does not present this transition.[19] Due to the molecular nature of both the electron-donor molecule and the charge-compensating anion in $(ET)_2[Fe(tdas)_2]$, the salt might be amenable to modification of its structure through chemical methods. It would be interesting to see if such modifications lead to solids in which the conduction electrons interact with the magnetic moments located at the anion layer.

Acknowledgements

Work at University of Cagliari is supported by CNR, Progetto "Materiali Speciali per Tecnologie Avanzate II". Work at Argonne National Laboratory is supported by the US-DOE under contract W-31-109-ENG-38. This research is carried out as part of a joint project supported by NATO with Collaborative Grant GRG951199. Work at North Carolina State University is supported by the U.S. Department of Energy, Office of Basic Sciences, Division of Materials Sciences, under grant DE-FG02-86ER45259. The authors thank Prof. A. Anedda and Dr S. Loi, Physics Department, University of Cagliari, for help with Raman measurements. Work at the Instituto de Ciencia Molecular of the Universidad de Valencia is sponsored by the Generalitat Valenciana and the Spanish Ministerio de Educación y Cultura (funding for purchase of the SQUID susceptometer) and the Spanish Ministerio de Ciencia y Tecnología (project MAT2001-3507-C02-01 and Italian–Spanish Integrated Action HI2000-76).

References

1 P. Day and M. Kurmoo, *J. Mater. Chem.*, 1997, **7**, 1291.
2 S. S. Turner, D. Le Pevelen, P. Day and K. Prout, *J. Chem. Soc., Dalton Trans.*, 2000, 2739.
3 E. Coronado, J. R. Galán-Mascarós, C. J. Gómez-García and V. Laukhin, *Nature*, 2000, **408**, 447.
4 E. Coronado and C. J. Gómez-García, *Chem. Rev.*, 1998, **98**, 273.
5 K. Awaga, E. Coronado and M. Drillon, *MRS Bull.*, 2000, 52.
6 H. Kobayashi, A. Kobayashi and P. Cassoux, *Chem. Soc. Rev.*, 2000, **29**, 325.
7 L. Ouahab, *Chem. Mater.*, 1997, **9**, 1909.
8 T. Ishiguro, K. Yamaji and G. Saito, *Organic Superconductors*, Springer-Verlag, Berlin, Heidelberg, New York, 2nd edn., 1998, vol. 88.
9 J. M. Williams, J. R. Ferraro, R. J. Thorn, K. D. Carlson, U. Geiser, H. H. Wang, A. M. Kini and M. H. Whangbo, *Organic Superconductors (Including Fullerenes)*, Prentice Hall, Englewood Cliffs, NJ, 1992.
10 M. Kurmoo, A. W. Graham, P. Day, S. J. Coles, M. B. Hursthouse, J. L. Caulfield, J. Singleton, F. L. Pratt, W. Hayes, L. Ducasse and P. Guionneau, *J. Am. Chem. Soc.*, 1995, **117**, 12209.
11 H. Tajima, M. Inokuchi, A. Kobayashi, T. Ohta, R. Kato, H. Kobayashi and H. Kuroda, *Chem. Lett.*, 1993, 1235.
12 A. T. Coomber, D. Beljonne, R. H. Friend, J. L. Brédas, A. Charlton, N. Robertson, A. E. Underhill, M. Kurmoo and P. Day, *Nature (London)*, 1996, **380**, 144.
13 P. Cassoux, L. Valade, H. Kobayashi, A. Kobayashi, R. A. Clark and A. E. Underhill, *Coord. Chem. Rev.*, 1991, **110**, 115.
14 F. Bigoli, P. Deplano, F. A. Devillanova, J. R. Ferraro, V. Lippolis, P. J. Lukes, M. L. Mercuri, M. A. Pellinghelli, E. F. Trogu and J. M. Williams, *Inorg. Chem.*, 1997, **36**, 1218.
15 F. Bigoli, P. Deplano, M. L. Mercuri, M. A. Pellinghelli, G. Pintus, E. F. Trogu, G. Zonnedda, H. H. Wang and J. M. Williams, *Inorg. Chim. Acta*, 1998, **273**, 175.
16 K. Awaga, T. Okuno, Y. Maruyama, A. Kobayashi, H. Kobayashi, S. Schenk and A. E. Underhill, *Inorg. Chem.*, 1994, **33**, 5598.
17 M. Takahashi, M. Takeda, K. Awaga, T. Okuno, Y. Maruyama, A. Kobayashi, H. Kobayashi, S. Schenk, N. Robertson and A. E. Underhill, *Mol. Cryst. Liq. Cryst.*, 1996, **286**, 77.
18 A. E. Underhill, N. Nobertson, J. Ziegenbalg, N. Le Narvor, J. D. Kilburn and K. Awaga, *Mol. Cryst. Liq. Cryst.*, 1996, **284**, 39.
19 N. Robertson, K. Awaga, S. Parsons, A. Kobayashi and A. E. Underhill, *Adv. Mater. Opt. Electron.*, 1998, **8**, 93.
20 L. Pilia, C. Faulmann, I. Malfant, V. Collière, M. L. Mercuri, P. Deplano and P. Cassoux, *Acta Crystallogr., Sect. C*, 2002, **58**, 240.
21 T. K. Hansen, J. Becher, T. Jorgensen, K. S. Varma, R. Khedekar and M. P. Cava, *Organic Synthesis*, 1995, **73**, 270.
22 K. S. Varma, A. Bury, N. J. Harris and A. E. Underhill, *Synthesis*, 1987, 837.
23 I. Hawkins and A. E. Underhill, *J. Chem. Soc., Chem. Commun.*, 1990, 1593.
24 T. J. Emge, H. H. Wang, M. A. Beno, J. M. Williams, M. H. Whangbo and M. Evain, *J. Am. Chem. Soc.*, 1986, **108**, 8215.
25 D. A. Stephens, A. E. Rehan, S. J. Compton, R. A. Barkhau and J. M. Williams, *Inorg. Synth.*, 1986, **24**, 135.
26 T. Mori, H. Mori and S. Tanaka, *Bull. Chem. Soc. Jpn.*, 1999, **72**, 179–197.
27 H. H. Wang, J. R. Ferraro, J. M. Williams, U. Geiser and J. A. Schlueter, *J. Chem. Soc., Chem. Commun.*, 1994, 1893.
28 H. H. Wang, B. A. Vogt, U. Geiser, M. A. Beno, K. D. Carlson, S. Kleinjan, N. Thorup and J. M. Williams, *Mol. Cryst. Liq. Cryst.*, 1990, **181**, 135.
29 H. H. Whangbo and R. Hoffmann, *J. Am. Chem. Soc.*, 1978, **100**, 6093.
30 J. Ren, W. Liang and M. H. Whangbo, *Crystal and Electronic Structure Analysis Using CAESAR*, PrimeColor Software, Inc., Raleigh, NC, USA, 1998 (http://www.PrimeC.com/).
31 M. H. Whangbo, *J. Chem. Phys.*, 1979, **70**, 4963.
32 M. H. Whangbo, H. J. Koo and K. S. Lee, *Solid State Commun.*, 2000, **114**, 27.
33 H. J. Koo and M. H. Whangbo, *J. Solid State Chem.*, 2000, **153**, 263.
34 H. J. Koo, M. H. Whangbo, S. Coste and S. Jobic, *J. Solid State Chem.*, 2001, **156**, 464.
35 H. J. Koo and M. H. Whangbo, *Inorg. Chem.*, 2001, **40**, 2161.
36 O. Kahn, *Molecular Magnetism*, VCH Publishers, New York, 1993.
37 A. P. Ginsberg and M. E. Lines, *Inorg. Chem.*, 1972, **11**, 2289.
38 J. C. Bonner and M. E. Fisher, *Phys. Rev. A*, 1964, **135**, 640.
39 D. B. Brown, J. A. Donner, J. W. Hall, S. R. Wilson, R. B. Wilson, D. J. Hodgson and W. E. Hatfield, *Inorg. Chem.*, 1979, **18**, 2635.
40 C. J. Gómez-García, C. Giménez-Saiz, S. Triki, E. Coronado, P. Le Magueres, L. Ouahab, L. Ducasse, C. Sourisseau and P. Delhaes, *Inorg. Chem.*, 1995, **34**, 4139.
41 E. Coronado, J. R. Galán-Mascarós, C. Giménez-Saiz, C. J. Gómez-García and S. Triki, *J. Am. Chem. Soc.*, 1998, **120**, 4671.
42 E. Coronado, J. R. Gálan-Mascarós, C. Giménez-Saiz, C. J. Gómez-García, C. Ruiz-Pérez and S. Triki, *Adv. Mater.*, 1996, **8**, 737.
43 M. Clemente-León, E. Coronado, J. R. Galán-Mascarós, C. J. Gómez-García and J. M. Fabre, *Synth. Met.*, 1999, **103**, 2279.
44 E. Coronado, J. R. Galán-Mascarós and C. J. Gómez-García, *J. Chem. Soc., Dalton Trans.*, 2000, 205.
45 S. Rashid, S. S. Turner, P. Day, M. E. Light and M. B. Hursthouse, *Inorg. Chem.*, 2000, **39**, 2426.
46 S. Triki, F. Bérézovsky, J. Sala Pala, A. Riou and P. Molinié, *Synth. Met.*, 1999, **103**, 1974.
47 S. Triki, F. Bérézovsky, J. S. Pala, C. J. Gómez-García, E. Coronado, K. Costuas and J.-F. Halet, *Inorg. Chem.*, 2001, **40**, 5127.